Morphology of early stage phase ordering

N. A. Gross
College of General Studies, Boston University, Boston, Massachusetts 02215

W. Klein
Department of Physics, Boston University and the Center for Computational Science, Boston, Massachusetts 02215

K. Ludwig
Department of Physics, Boston University, Boston, Massachusetts 02215

(Received 6 June 1997)

We present results of Monte Carlo simulations of critical quenches in Ising models with long range interactions indicating that linear theories of continuous ordering such as Cahn-Hilliard-Cook theory break down first at high wave numbers or small length scales. We connect this breakdown to the formation of isolated domains that resemble the stable phases. These domains grow and coalesce, causing deviations from the linear theory to appear at smaller wave numbers. When the domains of up (down) spins percolate the failure of the linear theory occurs on all length scales and the system has chosen the up (down) global magnetization state. [S1063-651X(97)02011-4]

PACS number(s): 64.60.Ak, 67.40.Fd

I. INTRODUCTION

Phase ordering kinetics occurs, for example, when a system undergoes a temperature quench from a disordered state above the critical temperature to a final state inside the coexistence curve [1]. If the order parameter is conserved, such as in binary alloy phase separation, this process is known as spinodal decomposition (SD). If the order parameter is not conserved and not coupled to a conserved quantity, which is the case when a system has undergone an order-disorder transition, this process is known as continuous ordering (CO). Both these processes are of technological interest to the materials science and metallurgy community; for example, alloys become embrittled when phase separation occurs [2,3]. On a fundamental level, the phase ordering process serves as an important test of our understanding of nonequilibrium dynamics. The goal of the work presented here is to describe the structures which form at early times in the processes and understand how they affect the evolution of the system.

The phase ordering process can be divided into several time regimes. At early times when the composition fluctuations are small, the dynamics are believed to be linear and characterized by exponential growth of composition fluctuations [4,5]. At late times, the system effectively consists of domains of the different phases separated by sharp interfaces. In this late stage regime, the domain growth is determined by the dynamics of the interfaces and characterized by dynamic scaling; that is, the domain morphology is invariant and can be described by a characteristic length scale that grows with time [6]. Aspects of both the early stage and the late stage seem to be well described theoretically: however, attempts at a crossover theory have met with little success. Perturbative expansions fail at about the same time as the linear theory [6] and other attempts such as those by Langer, Bar-on, and Miller [7] as well as Billotet and Binder [8] involve uncontrolled approximations. This paper is concerned with the limits of the early time regime at which the linear theory first fails to describe the evolution of the Fourier modes.

The linear theory for spinodal decomposition was introduced in 1959 by Cahn and Hilliard [4] and later extended by Cook to include thermal noise [5]. They predicted that at early times the composition fluctuations will grow exponentially at long wavelengths while the short wavelength modes relax to ''false'' equilibrium values. In 1984 Binder presented a Ginzburg-like consistency argument which stated that the linearized approximation is consistent for short times, but becomes inconsistent for time greater than some critical time t_c which scales with the range of interaction [9]. This is discussed further below. Although experiments [10,11] and simulations [12] agree with the linear Cahn-Hilliard-Cook (CHC) theory for certain parameter regimes, there are experimental indications that the linear predictions fail first on short length scales [10]. As we reported in a previous Letter [13], using Ising model simulations we have confirmed the observation that the linear theory fails first at short length scales. In addition we also presented evidence for the formation of dense domains whose size corresponds to length scales at which the linear theory has failed. We also showed that the linear theory fails on all length scales when the domains coalesce. In the current paper we show in detail how the linear theory fails to fit the simulation data at small length scales and present a generalized linear theory which, though it better describes the evolution of the order parameter, still fails in the same manner as the CHC theory. Finally, we study the structures of the domains which form on these length scales and discuss how they cause the failure of the linear theory.

The remainder of this paper is structured as follows. In Sec. II we review the linearized theory and attempts to predict the time at which it fails. In Sec. III the linear theory analysis of the simulation data is presented. The data are analyzed using both the standard CHC theory and a general-

ized linear theory. Though the generalized theory gives a better fit to the data using the same number of free parameters, evidence is presented which suggests that both theories fail on short length scales first. In Sec. IV a cluster mapping is used to identify growing domains of up (down) magnetization. We argue that these regions, which are of a size which is between an interaction range and a correlation length, are linked to the failure of linear theory on short length scales first.

II. REVIEW OF LINEAR THEORY

In this section we describe the linearized equation of motion for the order parameter $\phi(x,t)$ and structure factor $S(k,t)$ for the case of the nonconserved order parameter and present a consistency check to predict the time at which the linear theory is no longer a good approximation. Following Cahn and Hilliard and Cook [1,4,5], we begin with the Langevin equation [14]. When the order parameter is not conserved its equation of motion is

$$\frac{\partial}{\partial t}\,\phi(\vec{x},t) = -M\,\frac{\delta F}{\delta \phi} + \eta(\vec{x},t). \tag{2.1}$$

For the time scales considered in this work, the mobility M can be assumed to depend only on the temperature. η is uncorrelated Gaussian noise which satisfies the conditions

$$\langle \eta(\vec{x},t)\rangle = 0, \quad \langle \eta(\vec{x},t)\,\eta(\vec{x}',t')\rangle = M k_B T \delta(\vec{x}-\vec{x}')\,\delta(t-t'), \tag{2.2}$$

where T is the temperature and k_B is Boltzmann's constant. F is taken as the Ginzburg-Landau (GL) free energy with zero magnetic field.

$$F[\phi] = \int d\vec{x}\{R^2[\vec{\nabla}\phi(\vec{x},t)]^2 + \varepsilon\,\phi^2(\vec{x},t) + \phi^4(\vec{x},t)\}. \tag{2.3}$$

Here, R^2 is the second moment of the interaction potential, which can be taken as a measure of the interaction range, and the parameter $\varepsilon = (T-T_c)/T_c$ is the reduced temperature. If we insert Eq. (2.3) into Eq. (2.1) we get

$$\frac{\partial}{\partial t}\,\phi(\vec{x},t) = -M(-R^2\nabla^2\phi + 2\varepsilon\,\phi + 4\phi^3) + \eta(\vec{x},t). \tag{2.4}$$

This nonlinear equation has not been solved analytically; however, if we assume that $\phi(\vec{x},t)$ is small so that we can ignore the ϕ^3 term we obtain the linear Cahn-Hilliard-Cook equation.

$$\frac{\partial}{\partial t}\,\phi(\vec{x},t) = -M\{R^2[\nabla^2\phi(x,t)] + 2\varepsilon\,\phi(x,t)\} + \eta(\vec{x},t),$$

$$\frac{\partial}{\partial t}\,\tilde{\phi}(\vec{k},t) = -M(R^2k^2 + 2\varepsilon)\,\tilde{\phi}(k,t) + \tilde{\eta}(\vec{k},t), \tag{2.5}$$

where the second equation in Eq. (2.5) is the spatial Fourier transform of the first. The solution to the homogeneous equation [$\eta(\vec{x},t) = 0$] is

$$\phi(k,t) = \phi_0(k)\exp\{-M(R^2k^2 + 2\varepsilon)t\}, \tag{2.6}$$

which is simply the solution to the Cahn-Hilliard equation as originally presented in 1959 [4]. For $\varepsilon > 0$ Eq. (2.6) indicates that any perturbation will decay; however, if the system is quenched to below the critical temperature, then ε is negative and, for small wave vectors, $\phi(k,t)$ will grow. We can take the inverse Fourier transform of Eq. (2.6) to recover the real space configuration generated by this growth. In two dimensions we obtain

$$\phi(x,t) = \frac{\phi_0\pi}{2MR^2t}\,\exp\left(-2\varepsilon Mt - \frac{x^2}{4MtR^2}\right), \tag{2.7}$$

where we have assumed that $\phi_0(k)$ is a constant. This corresponds to an initial spatial configuration which is a δ function at the origin. Assuming that ε is negative the argument of the exponential can be rewritten as $[8|\varepsilon|M^2t^2 - (x/R)^2]/4Mt$. This suggests that at early times a growing domain has two growth fronts: a weak front which advances linearly with time, and a more robust front which advances like a random walk.

Equation (2.6) is the homogeneous solution of Eq. (2.5) and so it does not include the noise term η. In 1970, Cook obtained a form for the structure factor which included the noise [5]. To find the full solution to the CHC theory, we impose the causality condition and use the retarded Green function.

$$\tilde{\phi}(k,t) = \tilde{\phi}_0(k)\exp(-M\{R^2k^2 + 2\varepsilon\}t) + \int_0^t dt'\,\tilde{\eta}(k,t') \times \exp\{-M(R^2k^2 + 2\varepsilon)(t-t')\}. \tag{2.8}$$

By using the definition of the structure factor $S(k) = \langle|\tilde{\phi}(k)|^2\rangle$ along with the solution for the order parameter in Eq. (2.8) we can find the equation of motion for the structure factor $S(k,t)$.

$$\frac{\partial}{\partial t}\,S(k,t) = 2\left\langle\left|\,\tilde{\phi}(k,t)\,\frac{\partial}{\partial t}\,\tilde{\phi}(k,t)\right|\right\rangle,$$

$$\frac{\partial}{\partial t}\,S(k,t) = 2\langle|\,\tilde{\phi}(k,t)[-M(R^2k^2 + 2\varepsilon)\,\tilde{\phi}(k,t) + \tilde{\eta}(k,t)]|\rangle$$

$$= 2(MR^2k^2 + \varepsilon)\langle|\,\tilde{\phi}(k,t)|^2\rangle + 2\langle|\,\tilde{\phi}(k,t)\,\tilde{\eta}(k,t)|\rangle. \tag{2.9}$$

The first term in the last line of Eq. (2.9) is the equation of motion for the structure factor derived by Cahn and Hilliard [4]. Using Eq. (2.8), the second term yields

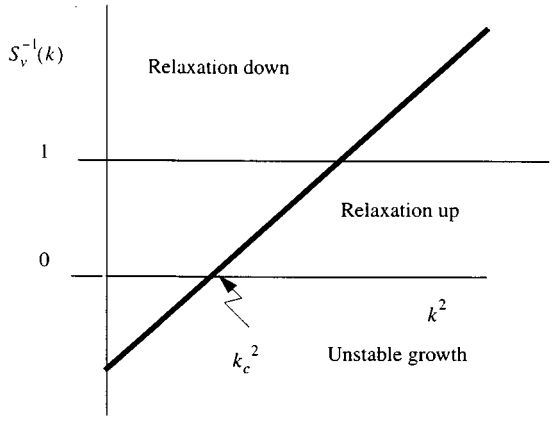

FIG. 1. Dynamic domains for CHC theory. The modes below k_c grow exponentially while those above k_c relax.

$$\langle|\tilde{\phi}(k,t)\,\tilde{\eta}(k,t)|\rangle=\int_0^t dt'\langle\tilde{\eta}(k,t')\,\tilde{\eta}(k,t)\rangle\exp\{M(R^2k^2+2\varepsilon)(t-t')\}$$
$$=Mk_bT\int_0^t dt'\,\delta(t-t')\times\exp\{M(R^2k^2+2\varepsilon)(t-t')\}$$
$$=Mk_bT. \tag{2.10}$$

The full equation of motion for the structure factor becomes

$$\frac{\partial}{\partial t}S(k,t)=-2M[R^2k^2-2|\varepsilon|]S(k,t)+2Mk_bT, \tag{2.11}$$

and its solution is

$$S(k,t)=[S(k,0)-S_\nu(k)]\exp\{-D(k)t\}+S_\nu(k),$$
$$S_\nu(k)=\frac{2k_bT}{R^2k^2-2|\varepsilon|},\quad D(k)=M[S_\nu(k)]^{-1}. \tag{2.12}$$

Equations (2.11) and (2.12) describe the CHC theory as presented by Cook in 1970 [5]. We have explicitly inserted a negative sign in front of the $|\varepsilon|$ and so Eq. (2.12) describes a system which has been quenched from a temperature above the critical point to a temperature below it. There are several features of this result which should be discussed and are illustrated in Fig. 1. In this figure the inverse of the CHC form of $S_v(\vec{k})$ has been plotted against k^2. First it should be noted that there is a critical wave vector where $S_v(\vec{k})$ changes sign. This is given by

$$R^2k_c^2-2|\varepsilon|=0\Rightarrow k_c=\sqrt{2|\varepsilon|}/R. \tag{2.13}$$

For wave vectors below k_c, $S_v(\vec{k})$ and $D(k)$ will be negative; so, for small wave vectors the argument of the exponential in Eq. (2.12) will be positive and the structure factor will grow exponentially. For wave vectors above k_c, the structure factor will relax exponentially towards $S_v(\vec{k})$.

If linear theory were exact, then the equilibrium structure factor would be $S_v(\vec{k})$. However, since $\int S(\vec{k},t)d\vec{k}$ is a conserved quantity (the system volume is a constant), exponential growth cannot go on indefinitely. For quenches to below T_c, the nonlinear terms in Eq. (2.4) will start to become important. At some time t_c the growth of structure factor at small wave vectors will be limited when the linear theory will fail to accurately describe the system. Note that if the system was above the critical point. $S_v(\vec{k})$ would always be positive and all wave vectors would relax exponentially to their equilibrium value which is given by $S_v(\vec{k})$. Thus, with the appropriate change of sign, we recover the Ornstein-Zernicke form of the structure factor for a system above the critical point.

Now that the properties of the linear theory have been discussed, we can consider when it is valid. As we have said, there exists a time t_c at which nonlinear terms become important and the linear theory must fail to describe the evolution of the structure factor. Before summarizing the arguments of Binder [9] which predict this breakdown time, we first need to review some scaling considerations.

Length scales smaller than the interaction range R should have very little significance for CHC theory, so we should be able to rescale all lengths with respect to the interaction range, $\phi(x)\rightarrow a\phi(x/R)$, however, we do not know the relation between a and R. Since the Langevin equation relates the time evolution of ϕ to the noise field η, we can use the scaling of η to uncover the scaling of ϕ.

For Gaussian random noise we have the relation

$$\langle\eta(\vec{x},t)\,\eta(\vec{x},t')\rangle=Mk_bT\delta(\vec{x}-\overline{x'})\,\delta(t-t'). \tag{2.14}$$

The scaling property of the δ function implies a scaling relation for the noise,

$$\frac{1}{R^d}\,\delta(\vec{x}/R)=\delta(\vec{x})\Rightarrow\frac{1}{R^{d/2}}\,\eta(\vec{x}/R,t)=\eta(\vec{x},t). \tag{2.15}$$

In linear theory we can assume that the field ϕ scales in the same way as the noise. This is consistent with the units of ϕ derived from the Ginzburg-Landau free energy given in Eq. (2.3). Assuming that the units of energy have been scaled away, then the integrand in Eq. (2.3) must have units of L^{-d}. Since ε in Eq. (2.3) is dimensionless, then ϕ must have dimensions of $L^{-d/2}$. When rescaling lengths by R we see that the field must have the scaling of the noise given in Eq. (2.15).

We can now outline a consistency check for linear theory. From Eq. (2.4) the linear theory should describe systems undergoing continuous ordering or spinodal decomposition as long as $\phi(\vec{x},t)>\phi(\vec{x},t)^3$ or $1>\phi(\vec{x},t)^2$. If we take $\phi_0(k)$ in Eq. (2.6) to be a Gaussian instead of flat as we assumed earlier then we can set the initial amplitude to be small enough so that the linear approximation holds for all k at zero time. Then the argument of the exponential equation (2.7) becomes

$$\frac{8|\varepsilon|Mt^2(MR^2+2\Delta)-x^2}{4t(MR^2+2\Delta)}. \tag{2.16}$$

Here Δ is the square of the inverse width of the initial Gaussian in k space. We see that the fastest growth occurs for small x and so this is where the consistency check should fail first. Inserting the scaling relationship for ϕ given in Eq. (2.15) into the solution to linear theory, it is possible to get a time scale beyond which linear theory is invalid.

$$\phi(0,t)=\frac{\exp(2M\varepsilon t_c)}{R^d}\cong 1\Rightarrow t_c=\frac{d}{2M\varepsilon}\ln(R). \quad (2.17)$$

t_c is weakly dependent on R which implies that linear theory is a good approximation for long range models. It is also strongly dependent on the distance from the critical point. This is consistent with the results of Binder [9], but Binder's argument does not indicate that the linear theory will fail on small length scales first. Note that this is a consistency check; the linear theory may still fail at times earlier than the critical time t_c obtained in Eq. (2.17). Another argument based on a supersymmetric representation of the CHC theory is given in Ref. [15] and predicts that the linear theory will fail on small length scales at times shorter than t_c. This was confirmed by the simulations done in our previous work [13]. Finally, Yeung, Gross, and Costolo [16] use mode slaving arguments to calculate the breakdown time for different Fourier modes and showed that $t_c(k)\sim k^{-2}$.

III. ANALYSIS OF THE STRUCTURE FACTOR DATA

In this section we present two different methods for using linear theory to analyze the structure factor data. The first method we present fits the structure factor to the explicit form of the CHC theory. For this method we are able to estimate the breakdown time as a function of wave number. We see that as the wave number increases the breakdown time gets smaller; thus the linear theory fails first at large wave numbers. The second method uses a more generalized linear theory. This method allows us to fit the data more closely for larger wave numbers. It still appears though that the linear theory will fail first at large wave numbers. The last section shows that the generalized theory is also useful in analyzing equilibrium data.

To test the prediction of the breakdown time for the linear theory simulations of the long range Ising model (LRIM) were used. In the LRIM a spin interacts with all of the other spins in a set region defined by some range R. In this work the region we chose is the square shown in Fig. 2. As the range is increased, the strength of the interaction is scaled by $1/R^d$ to keep the energy per spin finite [17]. For these models the physics depends only on the dimension of the system and the number of spins in the interaction range, which we will call q.

Once the interaction region is defined, it is possible to calculate the energy for the system.

$$E=-J\sum_i s_i \sum_{j\in I(s_i)} s_j. \quad (3.1)$$

Here $I(s_i)$ represents the set of spins in the interaction region of spin i. J is taken as one for the rest of this work. As $R\to\infty$ each spin interacts with more of its neighbors and this model approaches the mean field limit: though, for the model

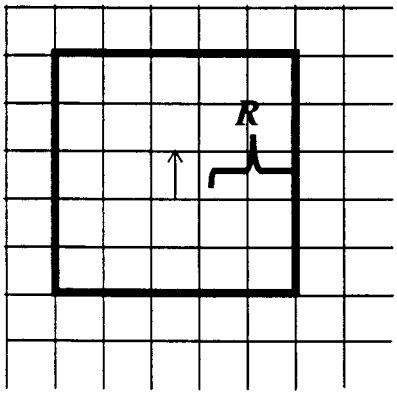

FIG. 2. This figure shows the geometry of the interaction region used in this work. The number of spins that a given spin interacts with is $q=(2R+1)^2-1$.

to be consistent, the thermodynamic limit should be taken before R is taken to infinity [17]. It was shown by Domb and Dalton [18] that the inverse critical temperature for this model scales with the interaction range and that scaling is given by

$$\beta_c=\frac{1}{q}\left(1+\frac{A}{q^\Gamma}\right), \quad (3.2)$$

where $A=3.7$ and $\Gamma=0.666$.

To explore the CHC theory thoroughly, systems of differing ranges and quench depths were investigated. First, all systems studied in this work start from an initial configuration of a random distribution of spins, which corresponds to a system in equilibrium at infinite temperature. Systems with interaction ranges of 7, 10, and 15 were quenched to an inverse temperature of $\beta=1.5$ in units where Boltzmann's constant is set equal to unity. Also, systems of range 7 were run at inverse temperatures varying between $\beta=1.2$ to $\beta=2.0$. Note that $\beta=1.0$ corresponds to the critical temperature for this system in the mean field ($R\to\infty$) limit. The exact critical temperature for the finite range systems used here differs from the mean field limit by only a few percent at most [18]. All systems are run on a two dimensional lattice, of size 512×512, with open boundary conditions. The boundary conditions are chosen to facilitate the cluster analysis which is discussed later in this work. A random update scheme was used to evolve the system [19]. For each set of parameters, 48 independent systems were run for four Monte Carlo steps (MCS). Configurations are saved every 1/32 of a MCS. For each of these times, the structure factor for each independent run was calculated. These are then averaged over the 48 runs and a circular average is calculated for the result so that the structure factor was only a function of the magnitude of the wave number. This process is done for each time step resulting in a time dependent structure factor $S(n,t)$, which can be compared to the predictions of the linear theory.

The structure factor data generated as described above can be fit with the explicit form of the CHC theory given in Eq. (2.12). In this form, k and t are the independent variables and k_bT/R^2, ε/R^2, and M are fitting parameters. Since linear theory is expected to fail at some finite time, the structure

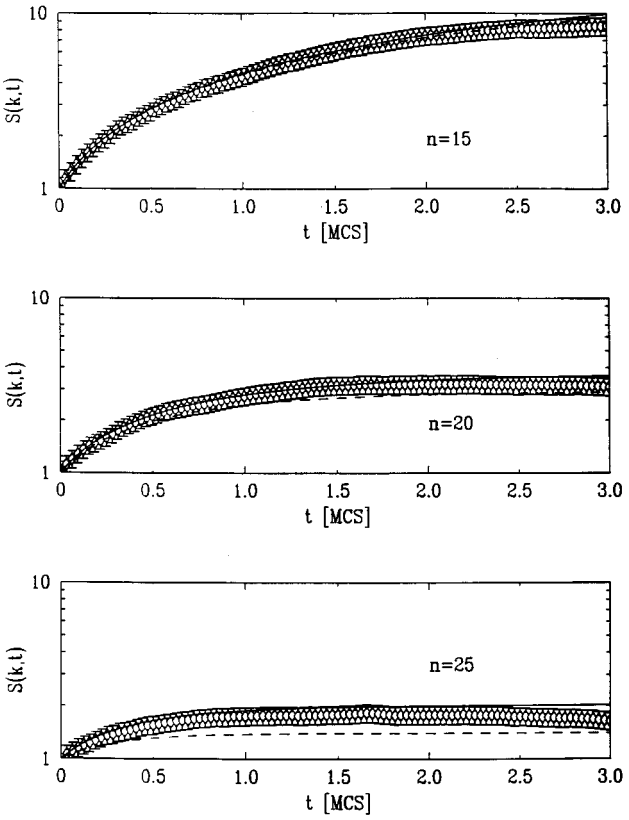

FIG. 3. Examples of the structure factor as a function of time for these simulations. The structure factor for three values of n are shown. The dotted line represents a fit to CHC theory while the solid line is a fit to the generalized linear theory. This is in units of $(k_bT)/J$ and J is taken as 1 in this work.

factor data were fit for some short time and then the fit was expanded to include all the data which were consistent with the preliminary fit. The fit was tried for the entire data set in an attempt to find a consistent set of fit parameters for all wave vectors. Figure 3 shows the results of this fit procedure for one set of data. The fit parameters are given in Table I and are consistent with expected results; however, it is clear that while the explicit form of the linear theory fits the data well for small wave numbers, consistent fits cannot be obtained for larger wave numbers for the same length of time. In fact, as the wave number increases, the time over which the fit is consistent with the data decreases.

The time at which the linear theory fails can be read off each graph and this time can be plotted against the wave number. This is exactly what has been done in Figs. 4 and 5. In Fig. 4 the data for several different quench depths are shown while Fig. 5 shows the data for different ranges of the interaction. Note that in Fig. 5 the wave number is scaled by the range so that the different data sets can be easily compared. All the data sets show the same trend; the breakdown time for small wave number is roughly constant and then drops off rapidly for larger wave number until it reaches a point where the CHC theory does not fit the data even at $t=0$. That is to say that the slope predicted by linear theory at $t=0$ is wrong for large wave number and so the nonlinear terms become important there first. As we will see later, the nonlinear terms manifest themselves as small compact do-

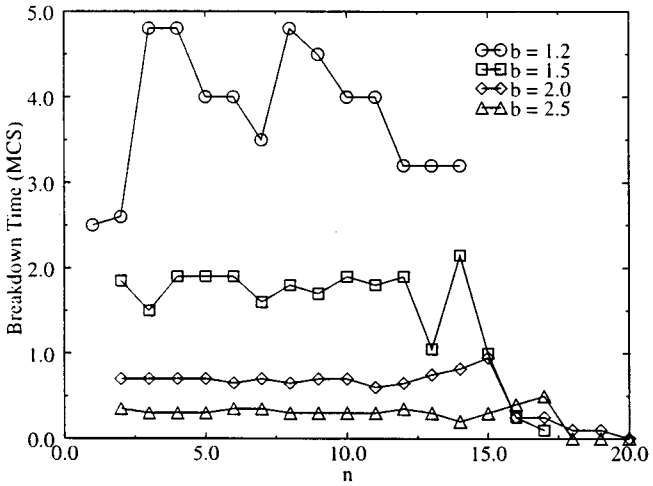

FIG. 4. The breakdown time for various quench depths and an interaction range of $R=7$.

mains in real space of either up or down spins which for large wave numbers become important to the structure factor calculation, but for small wave numbers appear to cancel each other out.

It is also possible to fit the structure factor to a generalized linear theory which includes higher order terms in the expansion of the interaction while still being able to decouple the modes. In fact Hopper and Uhlmann show that for many common interactions the higher order terms are important [20]. Consider the dynamic equation for the structure factor of the form

$$\frac{\partial}{\partial t} S(\vec{k},t) = -2MA(k)S(\vec{k},t) + 2Mk_bT. \tag{3.3}$$

Here M is a mobility, T is the temperature, and $A(k)$ is called the amplification factor which if set to $A(k)=-R^2k^2-2\varepsilon$ recovers Cahn-Hilliard-Cook theory. If this

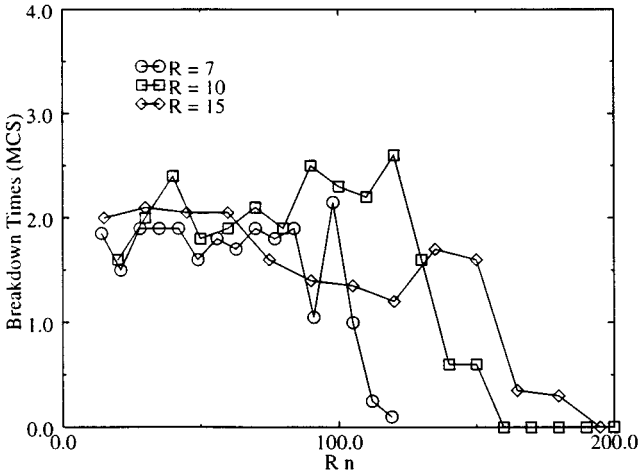

FIG. 5. The breakdown time for various interaction ranges and a quench depth of $\beta=1.5$.

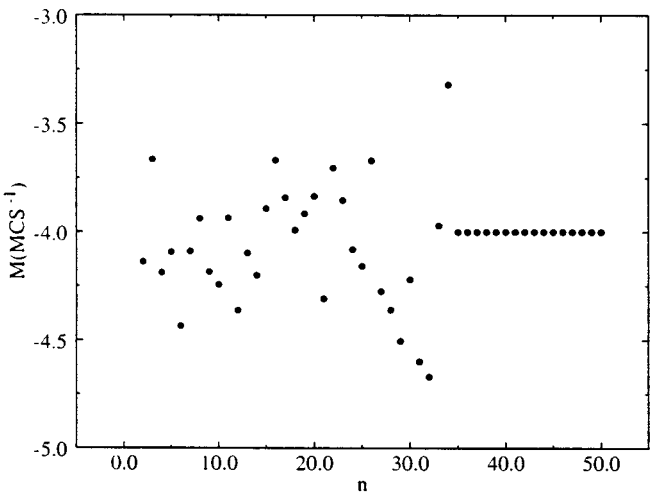

FIG. 6. The mobility as a function of wave number for $R=7$, $\beta=1.5$.

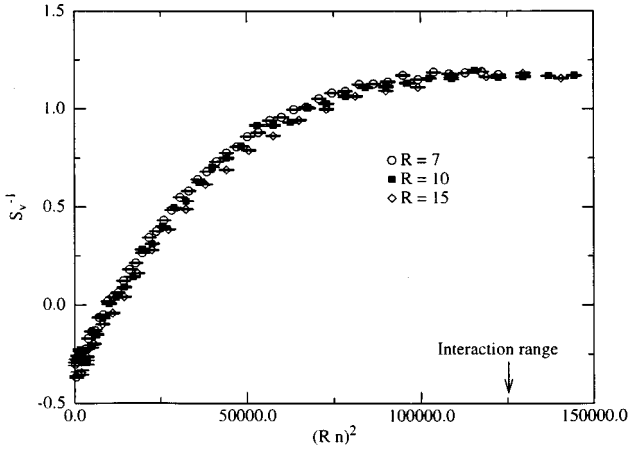

FIG. 7. The amplification factor as a function of $(Rn)^2$ for different interaction ranges. The amplification factor is unitless.

form of $A(k)$ is plotted against k^2, the resulting graph should show a linear relationship. In this section we show that if $A(k)$ is extracted from the time dependent structure factor, then $A(k)$ can be compared to the CHC form as well as other forms.

The solution to Eq. (3.3) is

$$S(\vec{k},t)=[S(\vec{k},0)-S_\nu(\vec{k})]\exp[-2MS_\nu^{-1}(\vec{k})t]+S_\nu(\vec{k}),$$

$$S_\nu(\vec{k})=k_bT/A(\vec{k}). \tag{3.4}$$

$S_v(k)$ is interpreted as the structure factor in equilibrium within the linear approximation; that is, when the linear theory is a reasonably good approximation, the structure factor evolves toward $S_v(k)$. Far above the critical point the linear theory is a good approximation and $S_v(k)$ is the equilibrium structure factor, while below the critical point the linear theory is only a good approximation for $k\ll 1$ and short times when the order parameter is small. In the latter case we will call $S_v(k)$ the virtual structure factor.

In Eq. (3.4) the scattering intensity of a particular wave vector does not depend on the amplitude of other wave vectors. Thus we can fit the data for each wave vector separately to a simple function of time. All of the runs in this work are temperature quenches from $T=\infty$ so the initial structure factor is that of a random configuration of spins, $S(k,0)=1$. Given these conditions we have only two fit parameters, M and $S_v(k)$, which can be varied to minimize the residuals.

The mobility M in Eq. (3.4) is defined as a dimensionless constant for Metropolis dynamics, though many investigators [21] absorb a factor k_bT making the mobility temperature dependent. Ludwig and Park [21] predicted that the mobility as defined in Eq. (3.3) should be 4. Figure 6 presents a plot of the mobility vs wave number. This plot shows that the mobility is independent of the wave number and is randomly distributed around 4. After $n=35$ the structure factor initially grows slowly, so the ''signal to noise ratio'' is fairly large. In order to fit to the form in Eq. (3.4) more easily, the mobility was held fixed at 4; hence, the constancy of M after $n=35$ shown in Fig. 6 has no meaning other than to signal beyond what point the mobility is fixed.

We can now study the amplification factor as a function of n for systems with different ranges of interactions and quenches to different temperatures. For large enough range the system should be well described by mean field theory and the physics should be independent of the range. In fact, as discussed above, it should be possible to rescale all lengths with R. When this is done, the wave number will rescale as $n\rightarrow Rn$. If we plot the amplification factor against Rn for systems which have different ranges but are quenched to the same temperature, the plots should collapse onto each other. Figure 7 shows a plot of the inverse of the virtual structure factor as a function of $(Rn)^2$. The data almost collapse to the same line. There is a slight offset in the y axis as the range increases. From the CHC form of the amplification factor we see that the y intercept is related to ε, the difference between the quench temperature and the critical point. Since T_c varies with R [18], the critical temperature of the system approaches 1 from below as the range gets larger. So, if different systems are quenched to the same temperature, the system with the larger range will be slightly further from the critical point.

If the CHC theory is correct, then the data plotted in Fig. 7 should be linear with n^2. Clearly Fig. 7 is not linear: though it may be possible to approximate $A(k)$ with a linear function of n^2 for small n, for larger n the amplification must have a functional form which includes higher orders of n^2. (Note that odd powers of n are excluded due to the symmetry of the potential.) The reader may be concerned that large n corresponds to length scales small enough to be on the order of the interaction range. To show that this is not the case, the wave number which corresponds to the interaction range, $n_i=(\text{lattice size})/R$, has been marked in Fig. 7. Notice that since all lengths in this figure have been scaled with R, this point is independent of the interaction range.

To explore the form of $A(n)$ more carefully, we can look at quenches to different temperatures. The amplification factor for different quenches is shown in Fig. 8. The data for three different temperatures are represented by different symbols. As in Fig. 7, the data shown in Fig. 8 can be fit to

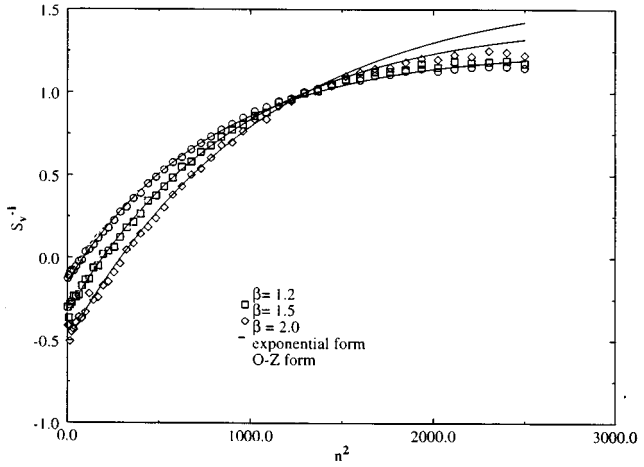

FIG. 8. The amplification factor as a function of n^2 for various quench depths. The amplification factor is unitless.

a function that is linear in n^2 for small values of n. However, for larger values of n, higher orders of n^2 are needed to fit the data. Each order introduces another parameter which should have some physical meaning unless all the parameters are related. If the parameters are related, then the CHC form may just be the first term in a Taylor series expansion of the correct form in which all orders of n^2 are present. For large n, $A(n)$ appears to go to a constant value. A form whose Taylor expansion is linear in n^2 and approaches a fixed value is the replacement $n^2 \rightarrow 1-\exp\{-R^2n^2\}$. We propose that the amplification factor in Eq. (3.4) is approximated by

$$A(n)=(1-\exp\{-R^2n^2\}-2\varepsilon) \tag{3.5}$$

rather than the CHC form. This form was used to fit the measured values of $A(n)$. These fits are represented by the curves in Fig. 8. The parameters for these fits are given in Table I. It should be noted that these are exactly the parameters which would be present in CHC theory. In fact, the dotted lines plotted in Fig. 8 represent $A(n)$ as predicted by CHC with the parameters given in Table I. Although it is better than the original CHC theory, the form for the amplification factor given in Eq. (3.5) does not correspond with the theory for high wave numbers. A careful examination of the data shows that it is not possible to fit the low and high wave numbers with exactly the same parameters. The data shown in Fig. 8 were only fit for the range $0<n^2<1500$. These fits still deviate for large n.

The deviation of the fit in Fig. 8 may imply that the form for $A(n)$ given in Eq. (3.5) is still incorrect but there exists a true linear theory for all wave numbers. One way to test this is to collect better statistics so that the noise in the scattering amplitude for higher wave numbers is smaller, and then use plots of $(d/dt)S(k,t)$ vs $S(k,t)$ to see if these higher wave numbers do indeed obey a linear theory. Note that because the potential used does not have circular symmetry, for these higher wave numbers the circular average used above is not a good approximation. The scattering amplitude is no longer a function of the magnitude of the wave vector, and each direction must be considered separately. Evidence for another form of S_ν will be given in the next section.

The results of the $(d/dt)S(k,t)$ vs $S(k,t)$ may also show that no form of linear theory is valid for large wave numbers; that is, all forms fail in a way similar to that shown for the CHC theory. Later in this paper other evidence for the failure of the linear theory at small length scales will be presented.

Although the form of $A(n)$ given in Eq. (3.5) may not be correct, it fits the data well enough to be suggestive. From Eq. (3.3) we see that $A(n)$ is the Fourier transform of the differential operator in front of $S(k,t)$ in the dynamical equation. From Eq. (3.3) we see that this is also the operator in front of ϕ in the Langevin equation and it is related to the functional derivative of the free energy. From above we see that higher orders of n^2 are important, indeed we may need all orders for a complete linear theory. In real space, the Langevin equation will then have to include all even derivatives of ϕ in order to be correct and the free energy must also include all even derivatives. If the true free energy includes higher order derivatives, then we should see their effect in equilibrium measurements. As discussed earlier, $S_\nu(k)$ would be the structure factor if the system were in equilibrium above the critical point. The relation to $A(k)$ is given in Eq. (3.4) and so the equilibrium structure factor has the form

$$S_\nu(n)=\frac{k_bT}{(1-\exp\{-R^2n^2\}+2\varepsilon)}. \tag{3.6}$$

Figure 9 shows the inverse of the measured structure factor for systems in equilibrium at the specified inverse temperature above the critical point. As with Fig. 7, the data sets in Fig. 9 are plotted against n^2. Again we see that this is not the linear relation predicted by the Ornstein-Zernicke form. The fits here are of the form given in Eq. (3.6). The fit parameters are given in Table II. Since these are equilibrium data, there is no dependence on dynamics. This form should only depend on the free energy. As discussed above, the free energy must include higher order derivatives.

Grewe and Klein have already derived $S(k)$ for the potential used in this work [22]. The potential used by Grewe and Klein is known as the Kac potential and is of the form

TABLE I. Parameters for fitting to the modified linear theory. Numbers in square brackets are powers of 10.

R	β	2ε	R^2	β
7	1.2	0.0903(0.0026)	0.001 11 (2.1[−5])	1.49 (0.014)
7	1.5	0.1891(0.0058)	0.001 08 (3.1 [−5])	1.773(0.022)
7	2.0	0.24 (0.013)	0.000 94 (4.7[−5])	2.139(0.039)
10	1.5	0.2226(0.0097)	0.002 506 (9.3 [−5])	1.647(0.02)
15	1.5	0.255 (0.0084)	0.005 45 (0.000 14)	1.722(0.015)

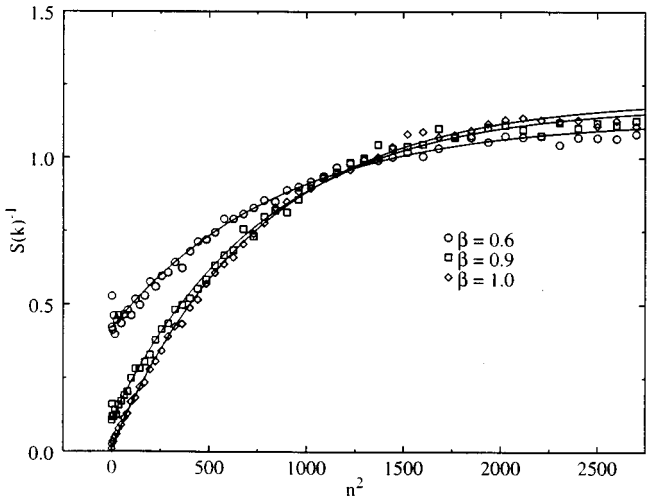

FIG. 9. Equilibrium structure factor plotted vs n^2 for various quench depths. This is in units of $(k_bT)/J$.

$V(x)=\gamma^d\phi(\gamma x)$. For our work $\gamma=1/R$ and ϕ is a step function in the form of a square as described in Sec. II. Notice that for this work the factor of $\gamma^d=1/q$ was initially associated with the inverse temperature but was scaled away. It then reappears in the potential. Grewe and Klein found that the inverse of the structure factor has the form

$$[S(\vec{k})]^{-1}=1-\beta\rho\tilde{L}(\vec{k}), \tag{3.7}$$

where β is the inverse temperature, ρ is the density of up spins, and $\tilde{L}(\vec{k})$ is the Fourier transform of the potential. In this work $\tilde{L}(\vec{k})$ is

$$\tilde{L}(\vec{k})=\left[\frac{\sin k_xR}{k_xR}\frac{\sin k_yR}{k_yR}\right]-2\varepsilon. \tag{3.8}$$

The last term in Eq. (3.8) comes from excluding the interaction of each spin with itself. Expanding Eq. (3.7) in a power series we can recover the Ornstein-Zernicke form for small wave vectors. Because of poor statistics and circularly averaged data it was not possible to compare the simulation results directly with the form of the structure factor derived by Grewe and Klein; however, the first few terms of the expansion of $\tilde{L}(\vec{k})$ are consistent with the first few terms of the proposed structure factor.

TABLE II. Parameters for equilibrium structure factors. Numbers in square brackets are powers of 10.

R	β	2ε	R^2	β
7	0.6	0.59(0.016)	0.001 173(6.1 [5])	0.711(0.013)
7	0.9	0.1013(0.0059)	0.001 284(3.4 [5])	1.074(0.01)
7	1.0	0.0116(0.004)	0.001 313(2.4 [5])	1.1888(0.0077)

IV. USING CLUSTERS TO EXPLORE THE EARLY TIME MORPHOLOGY

It has been shown above that the linear theory can be extended by including all orders of the interaction expansion. It is also argued above and in a previous paper that linear theory, as well as the extension, fail first not at large length scales, as would be concluded from the fact that $k=0$ is the fastest growing mode, but at small length scales. The remainder of this paper will be devoted to studying the structures which develop on small length scales and connecting the existence and growth of these domains to the breakdown of linear theory. These structures will be explored using a cluster mapping defined by Coniglio and Klein [23]; however, we shall first explore the cluster distribution which is present in the system at the time of the quench.

We have assumed throughout this work that the starting configuration is a lattice of random spins which corresponds to a system that is prepared at very high temperatures. Coniglio and Klein have shown that for a spin configuration which corresponds to a system in equilibrium there is a percolation transition at the critical temperature and that an infinite cluster which corresponds to the majority phase is present. In this section we will use simulations to show that, for a mean field system with a *random distribution* of spins, a percolation transition also occurs for the bond probability $p_b=1-e^{-2\beta}$ with β set to the inverse of the thermal critical temperature. In the mean field case there will be two infinite clusters, one for the up spins and one for the down spins.

In the mean field limit we can argue that a percolation transition exists for a random distribution of spins. If each spin interacts with q other spins then as q goes to infinity, the model approaches the mean field limit. We rescale all temperatures with respect to q so that $\beta\rightarrow\beta/q$ so that the rescaled thermal transition temperature corresponds to $\beta_c=1$. For large q the bond probability defined by Coniglio and Klein approaches $p_b=2\beta/q$. For a random configuration of spins only half of the spins $(q/2)$ which interact with a particular spin are in the same direction as that spin. Since, for mean field percolation, the critical bond probability is the inverse of the number of possible bonds, $p_c=2/q$, then with a random configuration of spins and the temperature set at that of the thermal transition, the Coniglio-Klein bond probability corresponds to the critical bond probability and so there exists a percolation transition.

It is possible to test these arguments via Monte Carlo simulations where the spin configuration is fixed, but many bond configurations are sampled. The percentage of bond configurations which contained spanning clusters can be plotted against β. Stauffer and Aharony argue that this function, which they call Π, is only a function of β and the lattice size L [24]. For an infinite lattice, Π is a step function with the step at β_c, while for finite lattices Π increases smoothly from zero below β_c, to unity above it. This is shown in Fig. 10 where Π is plotted against β for various values of the lattice size. The data shown are for an interaction range $R=7$. L varies from 128 to 512.

Stauffer and Aharony [24] suggest the form for Π is given by

$$\Pi=\Phi[(\beta-\beta_c)L^{1/\nu}]=C+\phi[(\beta-\beta_c)L^{1/\nu}], \tag{4.1}$$

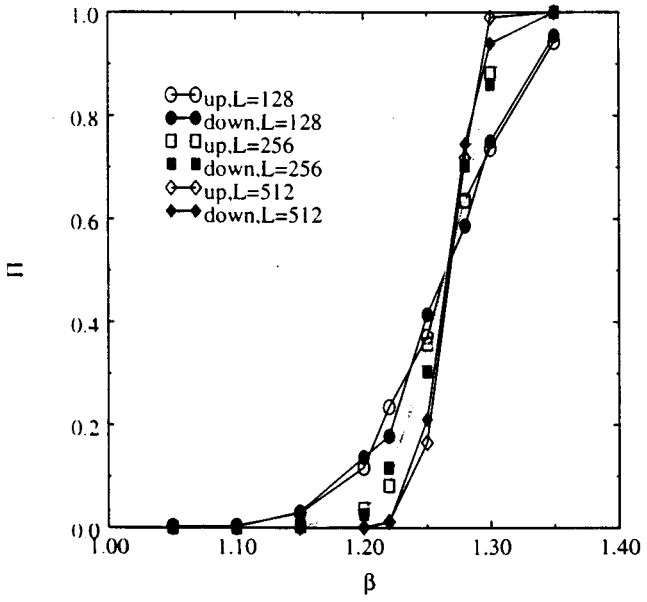

FIG. 10. Π vs the inverse temperature β for various lattice sizes. These curves intersect at the critical temperature.

where ϕ is an odd function around β_c and approaches $-C$ for small β and $(1-C)$ for large β. C is independent of the lattice size L so at $\beta=\beta_c$, $\Pi=C$ for any lattice size; thus at $\beta=\beta_c$ the curves for Π intersect. This can be used to find β_c. We see from Fig. 10 that β_c for this range of interaction is between 1.25 and 1.28.

Using the method described above, the percolation point was found for interaction ranges from $R=1$ to 15. To explore the scaling of the percolation transition the inverse temperature at which the transition occurs. β_p, can be plotted against q. We show this in Fig. 11, where we compare the scaling of the percolation transition to that of the thermal transition calculated by Domb and Dalton [18]. Both the lines shown are fits to the data using the Domb and Dalton form. The parameters for the fit of the percolation data are $\Gamma=-0.606(0.015)$ and $A=7.27(0.58)$. The slope is consistent with that of the slope of the thermal problem, $\Gamma=-0.666(0.068)$.

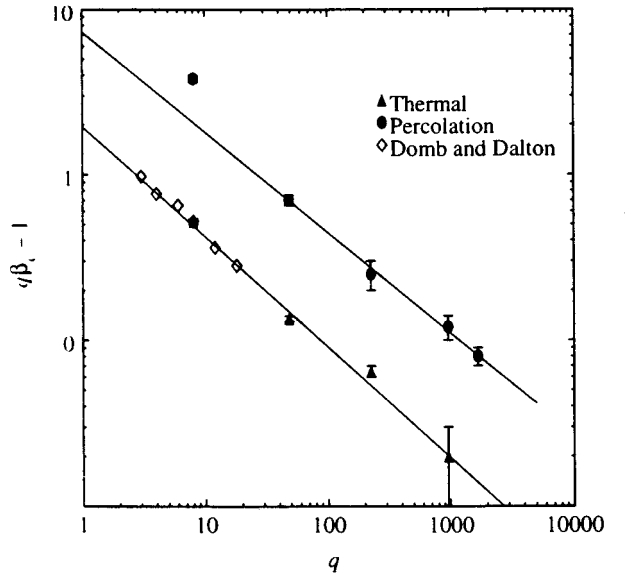

FIG. 11. Scaling of transition temperature with coordination number.

From these results we see that the critical temperature for the thermal problem and the critical temperature for percolation on a random lattice both scale in the same way with the coordination number, although the prefactor is different. Thus, for a sufficiently deep instantaneous quench below the critical point, initially there are two infinite clusters which are uniform over the lattice. If the system is quenched to a point below the thermal critical point but above the percolation transition no infinite clusters are initially present. Eventually, as the system evolves, only the equilibrium infinite cluster appears. The temperature region in which this occurs narrows as the interaction range increases (note that the scale in Fig. 11 is logarithmic) so that in the mean field limit, for any quench to a temperature below the critical point, two infinite clusters are present. We will see below that the two infinite clusters which appear can be used to follow the morphology of the system as it evolves. Eventually one of these infinite clusters will have to dissolve while the other fills in to become the equilibrium infinite cluster which corresponds to the magnetization. This suggests that there exists a ''mean field'' dynamics whose morphology is inherently different from dynamics of systems which are nonmean field. The dynamics of this morphology is what we will explore in the rest of this paper

To follow the evolution of the cluster structure, a single system is prepared at infinite temperature and allowed to evolve. At various time intervals the spin configuration will be frozen and a number of bond configurations will be sampled. Using the measured cluster properties we will observe the morphology of the system as a function of time. As the system evolves, structure can be identified by viewing the enhancement of the probability of belonging to the infinite cluster; that is, by visualizing the difference $P_\infty(x,t)-\langle P_\infty(x,0)\rangle$, where $P_\infty(x,t)$ is the probability that a spin at position x belongs to the infinite cluster at time t. Since the mapping identifies P_∞ with the magnetization, and the coarse grained magnetization is the order parameter for this problem, then the spatial fluctuations and evolution of P_∞ represent the spatial fluctuation and evolution of the order parameter. Since the initial configuration is a random uniform distribution which exhibits both an up and a down infinite cluster, these infinite clusters cancel each other, resulting in zero magnetization. This situation is much like that of a ''false vacuum.''

We will use the enhancements of P_∞ over its initial value to identify primitive domains in the system. Given the above arguments, we construct these enhanced regions in the following manner.

(1) The simulation is frozen at a particular time step, and for that particular spin configuration many configurations of the bonds are sampled. For each bond configuration it is noted which sites belong to the spanning cluster.
(2) $P_\infty(x,t)$ is estimated for each site by dividing the number of times that site belongs to the infinite cluster by the number of bond configurations sampled.

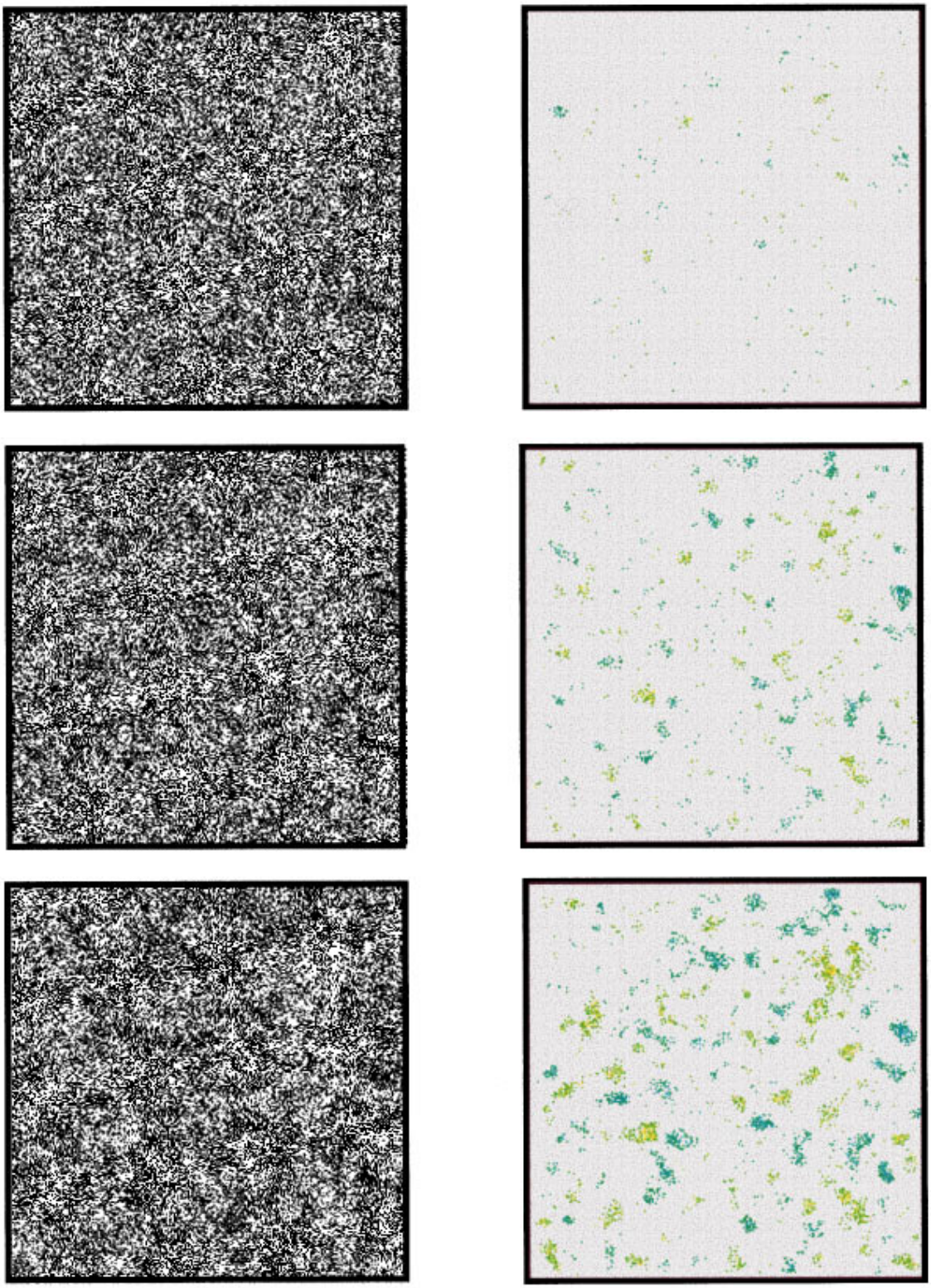

FIG. 12. (Color) Visual representations of the enhancements of spanning cluster. The figures on the left show the spin configuration at 0.5 MCS (top), 1.0 MCS (middle), and 1.5 MCS (bottom). Those on the right are a visualization of the enhancement of the infinite cluster using the procedure described in the text.

(3) The average value of P_∞ for the initial random configuration is calculated. For this configuration, P_∞ is nearly uniform over the system, having a small standard deviation. This standard deviation should go to zero as the range of interaction goes to infinity, i.e., as the system gets closer to the mean field limit. The value $P_{\mathrm{bg}} = \langle P_\infty(x,0)\rangle + 3\sigma[P_\infty(x,0)]$ is used as a background subtraction as $P_\infty(x,t)$ evolves. Here $\langle\cdots\rangle$ is the average over position and $\sigma[\cdots]$ is the standard deviation over position.

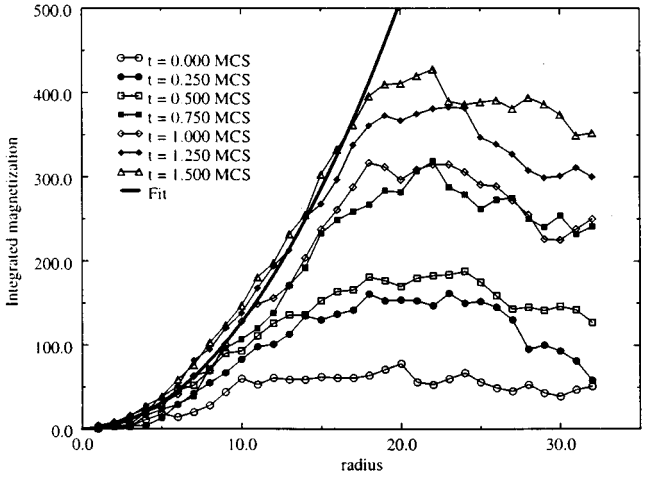

FIG. 13. The integrated magnetization of an enhance domain as a function of the distance from its center. This is simply the difference between the number of up spins and the number of down spins inside a radius r.

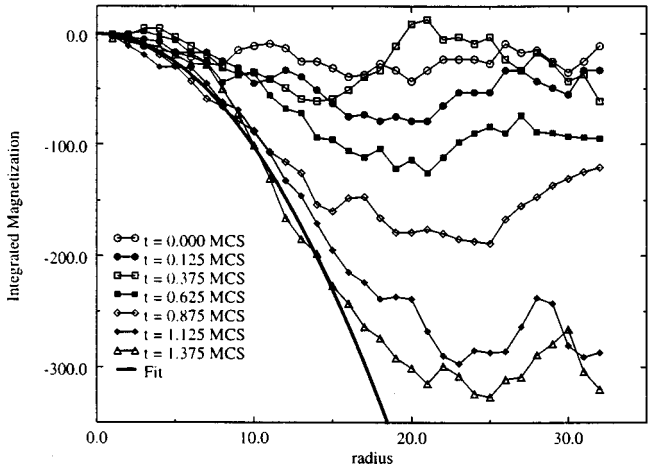

FIG. 14. The integrated magnetization of another domain in the vicinity of the one shown in Fig. 13.

(4) At each time step $P_\infty(x,t)-P_{\rm bg}$ is calculated. If this is less than zero, it is set to zero.

The visual realization of the procedure outlined above is shown in Fig. 12. In the third step above the value of three times the standard deviation was chosen so that no enhancement appears for the initial state. As the range is increased, the standard deviation will go to zero so that this cutoff is not needed in the mean field limit.

Now each site has associated with it a measure of how connected it is to one of the two spanning clusters and whether that connectivity has increased since the quench. To identify domains, we consider all spins of the same sign for which the measure is nonzero and which are within one interaction length of each other to be part of the same domain. Having done this we can identify the mass, center of mass, and radius of gyration of each domain. We will explore the domain profile in the next section and we will show that these domains have a significant magnetization as compared to the equilibrium magnetization, and that the domain boundaries are sharp. These domains were predicted in Ref. [15].

The domains shown in Fig. 12 appear to have distinct edges. To verify that this is actually the case the spin configuration itself can be analyzed. Using the center of mass of one of the domains the domain profile is constructed from the spin configuration by calculating the integrated magnetization inside a disk of a particular radius centered around the center of mass of a domain. From a plot of this integrated magnetization vs the radius the domain profile can be deduced. For the rest of the paper we will refer to such a plot as the domain profile. Figure 13 is just such a plot and shows the domain profile for a specific domain plotted at successive time steps. The dark solid line is a fit of the latest domain profile to a parabola. The profile of the domain at each time step exhibits similar behavior: that is, at each time step the integrated magnetization increases as the square of the radii up to a specific radius, and then the integrated magnetization is a constant. This signifies that the interiors of these domains have a uniform density of up spins which is greater than 50%, while the exterior still has a random distribution of up and down spins with a definite interface between interior and exterior. The fitted line shows that the density of up spins inside these domains is roughly half the equilibrium density, therefore in the interior of the droplets the order parameter is not small, so the evolution of the order parameter in the interior of these droplets should not obey a linear theory.

Figure 14 shows the profile of another domain which is adjacent to the domain whose profile is given in Fig. 13. Notice that for large radius both profiles start to decrease. The two domains shown are of opposite sign, and the decrease at large r is the contribution of the other domain to the sum. In the case of Fig. 14 we see the effects of even a third domain, this time of the same sign, causing the integrated magnetization to start increasing after it has started to decrease. This is confirmed by detailed analysis of the domain configurations generated by the procedure described above.

At a time slightly greater than one MCS these domains begin to interact. Domains of the same sign will start to coalesce, while domains of different signs form phase boundaries. The coalescence of domains can be seen by plotting the number of domains as a function of time. Figure 15 shows this effect. Here we see three sets of data for different interaction ranges all run at $\beta=1.5$. The scaled density is the total number of domains divided by the volume of the system measured in interaction volumes (that is, the volume of the system divided by the volume of an interaction region). The first thing to note is that the cluster density scales with the interaction range in the obvious way, that is, once the volume is rescaled the density is independent of range. Up to one MCS the number of domains is increasing as new domains form. At one MCS the domains start to interact and coalesce, though new domains must also be forming because the domain density (the number of domains per unit volume) stays constant for a short time. The domain density begins to decrease after 1.5 MCS, signifying that no new domains are forming; any fluctuations that do happen occur either inside of or within one interaction range of a domain which is already present. The domain density decreases after 1.5 MCS as the domains continue to coalesce.

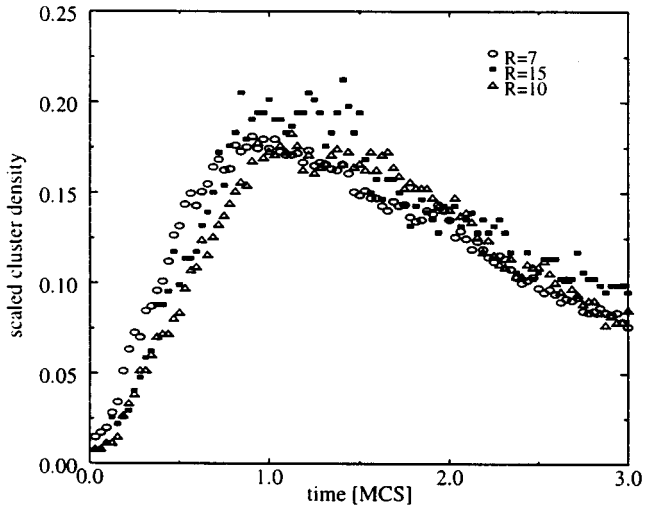

FIG. 15. Scaled domain density as a function of time from different interaction ranges.

It is possible to predict the growth rate of the domain density for the early times using arguments first proposed by Ray, Tamayo, and Klein [25]. These authors show that, for a mean field system in equilibrium, the time dependence of the magnetization can be modeled as a random walk in magnetization space. This argument should apply for regions which have not reached threshold, that is, for regions which contain no domains. Regions which have reached threshold are no longer doing an unbiased random walk and are trapped in the well into which they have fallen. We are able then to calculate the percentage of regions which have passed the threshold at a given time.

In the continuum limit, a random walk can be described by a diffusion equation. To model the case in question, absorbing boundary conditions will be used to account for the regions which have exited the top of the hill and are no longer performing a random walk. We can solve the diffusion equation with these conditions along with the appropriate initial conditions and find the percentage of domains which are no longer inside the boundaries as a function of time. If $P(m,t)$ is the percentage of interaction region with magnetization m at time t then the diffusion equation is

$$\frac{d}{dt}P(m,t)=\frac{d^2}{dm^2}P(m,t). \tag{4.2}$$

For absorbing boundaries at magnetization at $\pm M$, the solution to Eq. (4.2) is

$$P(m,t)=\sum_n A_n \cos\left(\frac{\pi m(2n+1)}{2M}\right) \times\exp\left[-t\left(\frac{\pi m(2n+1)}{2M}\right)^2\right]. \tag{4.3}$$

The initial conditions will set the value of A_n. Initially the magnetization of each interaction range is distributed in a normal Gaussian distribution. Note that the probability that a spin belongs to the infinite cluster is related to the number of interacting neighbors that spin has in the same direction as the spin. So the initial distribution of interaction region magnetizations is

$$P(m,0)=\frac{1}{(2\pi\sigma)^{1/2}}\exp\left(\frac{-m^2}{2\sigma}\right), \tag{4.4}$$

where σ is the spread of the initial distribution. The coefficients A_n then become

$$A_n=\frac{1}{2\sigma}\exp\left[-2\sigma\left(\frac{\pi(2n+1)}{2M}\right)^2\right], \tag{4.5}$$

and the probability distribution becomes

$$P(m,t)=\sum_n \frac{1}{2\sigma}\exp\left[-(2\sigma+t)\left(\frac{\pi m 2n+1}{2M}\right)^2\right] \times\cos\left(\frac{\pi m(2n+1)}{2M}\right). \tag{4.6}$$

We want to know the percentage of domains which have passed through the boundaries. This can be found from the percentage of domains which are still contained in the boundaries.

$$\int_{-M}^{M}P(m,t)dm=\frac{4M}{2\sigma\pi}\sum_n \frac{1}{(2n+1)}\exp\left[-(2\sigma+t) \times\left(\frac{\pi 2n+1}{2M}\right)^2\right]. \tag{4.7}$$

The number of domains that have passed the threshold then is $D(t)=1-\int_{-L}^{L}P(m,t)$. Since the argument of the exponential for $n=1$ is nearly an order of magnitude bigger than that for $n=0$, we can drop all the higher order terms and only look at the $n=0$ term in this sum. Since we are only interested in short times, we expand this term in a power series and look at the leading orders.

$$D(t)\approx 1-\frac{4M}{2\sigma\pi}\left[1-\left(\frac{\pi}{2M}\right)^2(2\sigma+t)\right]. \tag{4.8}$$

We see in Eq. (4.8) that for short times the number of domains that will be above threshold grows linearly with time. Looking at Fig. 15 this is exactly what we observe.

V. SOME CONCLUDING REMARKS

The aim of the work presented above was to understand the breakdown of the linear theory, which at best describes the early stage continuous ordering and spinodal decomposition. A simple analysis of the spatial structures predicted by the CHC theory shows that compact domains will form on small length scales and the order parameter inside these domains will quickly grow so that the linear theory will no longer be valid in the interior of these domains. The time associated with the failure of the linear theory within these domains scales as $\ln(R)/\varepsilon$ consistent with the predictions of Binder [9]. Our simulations have confirmed part of this picture, however, there are subtle but important differences. It is important to note that the simple analysis of the CHC equa-

tion, as well as Binder's construction of the Ginzburg criterion, are consistency checks and do not rule out that the CHC theory will fail on shorter time scales.

In fact, we have shown both here and in a previous work [13] that the linear theory fails first on short length scales. We did this by comparing the structure factor measured from Ising model simulations to the structure factor predicted by linear theory. We presented data which confirmed that the breakdown time was a function of the wave number and decreased with higher wave numbers. This was true even when we included the details of the interaction energy in a generalized linear theory. However, the scaling of the breakdown time with R and ε was not confirmed.

It is also interesting to note that the system appears to ''decide''which well it will go into when the domains percolate. In every case when the up domains percolate the system goes into the up magnetization well. The same process occurs with the opposite sign when the down spin domains percolate. We have also tested this by taking a system to completion and noting which well it has chosen. We then rerun the system with the same initial conditions and same noise field (same random number seed). At several time intervals we stop the evolution, make several identical copies, and restart each copy with different noise. If the various copies are made before the domains have coalesced then half of the copies will fall into the up well while the other half will fall into the down. On the other hand, if we perform this process after domain coalescence, all the copies will fall into the same well. Note that domain coalescence occurs early in the evolution of the system.

In the second half of this work we mapped the Ising model onto a percolation model to identify growing domains of up and down spins which are surrounded by a sea of randomly distributed spins. The random distribution is expected since the system was equilibrated at T_∞ prior to the quench. The order parameter in the interior of these domains is quite large, comparable with the equilibrium value, and so a linearized theory should no longer be valid in the interior. The order parameter in the exterior of these domains is still small and so the linear theory should still be valid on length scales larger than the average domain size. We found that the size of the domains appears to coincide with the length scale at which linear theory has failed and we have shown in a previous publication [13] that the linear theory fails on all length scales when the domains of either the up or down spins percolate and hence span the system. The difference between this result and the consistency checks discussed above is that any growth associated with the instability appears on a time scale of ε^{-1} *independent of* R. The R dependence appears in the time scale associated with the percolation of domains. Since the breakdown of linear theory has been connected to the growth of compact isolated domains, any nonlinear theory will have to account for them. This is not done for theories such as those of Langer, Bar-on, and Miller [7] or Billotet and Binder [8].

ACKNOWLEDGMENTS

The authors would like to thank Richard Brower and Harvey Gould for many useful conversations and Robert Putnam for technical assistance. This work was supported by Grant Nos. DMR-9633385 and DMR-9633596 from the National Science Foundation.

[1] J. W. Cahn, Acta Metall. **9**, 795 (1967); Trans. Metall. Soc. AIME **242**, 165 (1968), and references therein.

[2] A. Cerezo, M. G. Hetherington, J. M. Hyde, and M. K. Miller, Scr. Metall. Mater. **25**, 1435 (1991); also an article by the same authors published in *Alloy Phase Stability and Design*, edited by G. M. Stocks, D. P. Pope, and A. F. Giamei, MRS Symposia Proceedings No. 186 (Materials Research Society, Pittsburgh, 1991), p. 203.

[3] M. K. Miller and G. D. W. Smith, MRS Bull. **19**(7), 24 (1994).

[4] J. W. Cahn and J. E. Hilliard, J. Chem. Phys. **31**, 688 (1959).

[5] H. E. Cook, Acta Metall. **18**, 297 (1970).

[6] J. D. Gunton, M. San Miguel, and P. S. Sahni, in *Phase Transitions and Critical Phenomena*, edited by C. Domb and J. L. Lebowitz (Academic, New York, 1983), Vol. 8; H. Furukawa, Adv. Phys. **34**, 703 (1985); A. J. Bray, *ibid.* **43**, 357 (1994).

[7] J. S. Langer, M. Bar-on, and H. D. Miller, Phys. Rev. A **11**, 1417 (1975). This is also reviewed by D. Gunton, M. S. Miguel, and P. S. Sahni, in *Phase Transitions and Critical Phenomena*, edited by C. Domb and J. L. Lebowitz (Academic, New York, 1983), Vol. 8.

[8] C. Billotet and K. Binder, Z. Phys. B **32**, 195 (1979).

[9] K. Binder, Phys. Rev. A **29**, 341 (1984).

[10] F. S. Bates and P. Wiltzius, J. Chem. Phys. **91**, 3258 (1989); T. Izumitani and P. Hashimoto, *ibid.* **87**, 3694 (1985); B. D. Gaulin, S. Spooner, and Y. Morii, Phys. Rev. Lett. **59**, 668 (1987); A. E. Bailey and D. S. Cannell *ibid.* **70**, 2110 (1993).

[11] Y. Xie, Ph.D. dissertation, UNIVERSITY, 1994.

[12] M. Laradji, M. Grant, M. J. Zuckermann, and W. Klein, Phys. Rev. B **41**, 4646 (1990); K. R. Elder, T. M. Rogers, and R. C. Desai, *ibid.* **38**, 4725 (1988).

[13] N. Gross, W. Klein, and K. Ludwig, Phys. Rev. Lett. **73**, 2639 (1994).

[14] See, for example, S. R. de Groot and P. Mauzur, *Non-Equilibrium Thermodynamics* (Dover, New York, 1984) p. 119.

[15] W. Klein and G. G. Batrouni, Phys. Rev. Lett. **67**, 1278 (1991).

[16] C. Yeung, N. Gross, and M. Costolo, Phys. Rev. E **52**, 6025 (1995).

[17] M. Kac, G. E. Uhlenbeck, and P. C. Hemmer, J. Mod. Phys. **4**, 216 (1961).

[18] C. Domb and N. Dalton, Proc. Phys. Soc. London **89**, 859 (1966).

[19] N. A. Gross, Ph.D. thesis, Boston University, 1994; D. W. Heermann and A. N. Burkitt, *Parallel Algorithms in Computational Science* (Springer-Verlag, Berlin, 1991).

[20] R. W. Hopper and D. R. Uhlmann, Acta Metall. **21**, 377 (1973).

[21] K. Ludwig and B. Park Phys. Rev. B **46**, 5079 (1992).

[22] N. Grewe and W. Klein, J. Math. Phys. (N.Y.) **18**, 1729 (1977).
[23] A. Coniglio and W. Klein J. Phys. A **13**, 2775 (1980).
[24] D. Stauffer and A. Aharony, *Introduction to Percolation Theory* (Taylor and Francis, London, 1992).
[25] T. S. Ray, P. Tamayo, and W. Klein, Phys. Rev. A **39**, 5949 (1989).